EUROPEAN ORGANISATION FOR NUCLEAR RESEARCH

A measurement of the QCD colour factor ratios C_A/C_F and T_F/C_F from angular correlations in four-jet events

The OPAL Collaboration

Abstract

From 1 105 045 hadronic Z^0 decays observed with the OPAL detector at the LEP e^+e^- collider, 21 732 four-jet events are selected. A simultaneous fit of three selected angular variables from these events by the second order QCD matrix element calculation yields

$$C_A/C_F = 2.11 \pm 0.16(\text{stat.}) \pm 0.28(\text{syst.})$$

$$T_F/C_F = 0.40 \pm 0.11(\text{stat.}) \pm 0.14(\text{syst.})$$

for the ratios of colour factors, in agreement with SU(3) expectations of $C_A/C_F = 9/4$ and $T_F/C_F = 3/8$.

(Submitted to Physics Letters B)

The OPAL Collaboration

R. Akers[16], G. Alexander[23], J. Allison[16], K.J. Anderson[9], S. Arcelli[2], S. Asai[24], A. Astbury[28],
D. Axen[29], G. Azuelos[18,a], A.H. Ball[17], E. Barberio[26], R.J. Barlow[16], R. Bartoldus[3],
J.R. Batley[5], G. Beaudoin[18], A. Beck[23], G.A. Beck[13], J. Becker[10], C. Beeston[16], T. Behnke[27],
K.W. Bell[20], G. Bella[23], P. Bentkowski[18], S. Bentvelsen[8], P. Berlich[10], S. Bethke[32], O. Biebel[32],
I.J. Bloodworth[1], P. Bock[11], H.M. Bosch[11], M. Boutemeur[18], S. Braibant[12], P. Bright-Thomas[25],
R.M. Brown[20], A. Buijs[8], H.J. Burckhart[8], C. Burgard[27], P. Capiluppi[2], R.K. Carnegie[6],
A.A. Carter[13], J.R. Carter[5], C.Y. Chang[17], C. Charlesworth[6], D.G. Charlton[8], S.L. Chu[4],
P.E.L. Clarke[15], J.C. Clayton[1], S.G. Clowes[16], I. Cohen[23], J.E. Conboy[15], M. Coupland[14],
M. Cuffiani[2], S. Dado[22], C. Dallapiccola[17], G.M. Dallavalle[2], C. Darling[31], S. De Jong[13],
H. Deng[17], M. Dittmar[4], M.S. Dixit[7], E. do Couto e Silva[12], J.E. Duboscq[8], E. Duchovni[26],
G. Duckeck[8], I.P. Duerdoth[16], U.C. Dunwoody[5], P.A. Elcombe[5], P.G. Estabrooks[6], E. Etzion[23],
H.G. Evans[9], F. Fabbri[2], B. Fabbro[21], M. Fanti[2], M. Fierro[2], M. Fincke-Keeler[28], H.M. Fischer[3],
P. Fischer[3], R. Folman[26], D.G. Fong[17], M. Foucher[17], H. Fukui[24], A. Fürtjes[8], P. Gagnon[6],
A. Gaidot[21], J.W. Gary[4], J. Gascon[18], N.I. Geddes[20], C. Geich-Gimbel[3], S.W. Gensler[9],
F.X. Gentit[21], T. Geralis[20], G. Giacomelli[2], P. Giacomelli[4], R. Giacomelli[2], V. Gibson[5],
W.R. Gibson[13], J.D. Gillies[20], J. Goldberg[22], D.M. Gingrich[30,a], M.J. Goodrick[5], W. Gorn[4],
C. Grandi[2], P. Grannis[8], E. Gross[26], J. Hagemann[27], G.G. Hanson[12], M. Hansroul[8],
C.K. Hargrove[7], J. Hart[8], P.A. Hart[9], M. Hauschild[8], C.M. Hawkes[8], E. Heflin[4],
R.J. Hemingway[6], G. Herten[10], R.D. Heuer[8], J.C. Hill[5], S.J. Hillier[8], T. Hilse[10], D.A. Hinshaw[18],
P.R. Hobson[25], D. Hochman[26], A. Höcker[3], R.J. Homer[1], A.K. Honma[28,a], R.E. Hughes-Jones[16],
R. Humbert[10], P. Igo-Kemenes[11], H. Ihssen[11], D.C. Imrie[25], A. Jawahery[17], P.W. Jeffreys[20],
H. Jeremie[18], M. Jimack[1], M. Jones[6], R.W.L. Jones[8], P. Jovanovic[1], C. Jui[4], D. Karlen[6],
K. Kawagoe[24], T. Kawamoto[24], R.K. Keeler[28], R.G. Kellogg[17], B.W. Kennedy[20], B. King[8],
J. King[13], S. Kluth[5], T. Kobayashi[24], M. Kobel[10], D.S. Koetke[8], T.P. Kokott[3], S. Komamiya[24],
R. Kowalewski[8], R. Howard[29], P. Krieger[6], J. von Krogh[11], P. Kyberd[13], G.D. Lafferty[16],
H. Lafoux[8], R. Lahmann[17], J. Lauber[8], J.G. Layter[4], P. Leblanc[18], P. Le Du[21], A.M. Lee[31],
E. Lefebvre[18], M.H. Lehto[15], D. Lellouch[26], C. Leroy[18], J. Letts[4], L. Levinson[26], Z. Li[12], F. Liu[29],
S.L. Lloyd[13], F.K. Loebinger[16], G.D. Long[17], B. Lorazo[18], M.J. Losty[7], X.C. Lou[8], J. Ludwig[10],
A. Luig[10], M. Mannelli[8], S. Marcellini[2], C. Markus[3], A.J. Martin[13], J.P. Martin[18],
T. Mashimo[24], P. Mättig[3], U. Maur[3], J. McKenna[29], T.J. McMahon[1], A.I. McNab[13],
J.R. McNutt[25], F. Meijers[8], F.S. Merritt[9], H. Mes[7], A. Michelini[8], R.P. Middleton[20],
G. Mikenberg[26], J. Mildenberger[6], D.J. Miller[15], R. Mir[26], W. Mohr[10], C. Moisan[18],
A. Montanari[2], T. Mori[24], M. Morii[24], U. Müller[3], B. Nellen[3], B. Nijjhar[16], S.W. O'Neale[1],
F.G. Oakham[7], F. Odorici[2], H.O. Ogren[12], C.J. Oram[28,a], M.J. Oreglia[9], S. Orito[24],
J.P. Pansart[21], G.N. Patrick[20], M.J. Pearce[1], P. Pfister[10], P.D. Phillips[16], J.E. Pilcher[9],
J. Pinfold[30], D. Pitman[28], D.E. Plane[8], P. Poffenberger[28], B. Poli[2], A. Posthaus[3],
T.W. Pritchard[13], H. Przysieczniak[18], M.W. Redmond[8], D.L. Rees[8], D. Rigby[1], M. Rison[5],
S.A. Robins[13], D. Robinson[5], J.M. Roney[28], E. Ros[8], S. Rossberg[10], A.M. Rossi[2], M. Rosvick[28],
P. Routenburg[30], Y. Rozen[8], K. Runge[10], O. Runolfsson[8], D.R. Rust[12], M. Sasaki[24], C. Sbarra[2],
A.D. Schaile[8], O. Schaile[10], F. Scharf[3], P. Scharff-Hansen[8], P. Schenk[4], B. Schmitt[3], H. von der
Schmitt[11], M. Schröder[12], H.C. Schultz-Coulon[10], P. Schütz[3], M. Schulz[8], C. Schwick[27],
J. Schwiening[3], W.G. Scott[20], M. Settles[12], T.G. Shears[5], B.C. Shen[4],

C. H. Shepherd-Themistocleous[7], P. Sherwood[15], G. P. Siroli[2], A. Skillman[16], A. Skuja[17], A. M. Smith[8], T. J. Smith[28], G. A. Snow[17], R. Sobie[28], R. W. Springer[17], M. Sproston[20], A. Stahl[3], C. Stegmann[10], K. Stephens[16], J. Steuerer[28], B. Stockhausen[3], R. Ströhmer[11], D. Strom[19], P. Szymanski[20], H. Takeda[24], T. Takeshita[24], S. Tarem[26], M. Tecchio[9], P. Teixeira-Dias[11], N. Tesch[3], M. A. Thomson[15], S. Towers[6], T. Tsukamoto[24], M. F. Turner-Watson[8], D. Van den plas[18], R. Van Kooten[12], G. Vasseur[21], M. Vincter[28], A. Wagner[27], D. L. Wagner[9], C. P. Ward[5], D. R. Ward[5], J. J. Ward[15], P. M. Watkins[1], A. T. Watson[1], N. K. Watson[7], P. Weber[6], P. S. Wells[8], N. Wermes[3], B. Wilkens[10], G. W. Wilson[4], J. A. Wilson[1], V-H. Winterer[10], T. Wlodek[26], G. Wolf[26], S. Wotton[11], T. R. Wyatt[16], A. Yeaman[13], G. Yekutieli[26], M. Yurko[18], W. Zeuner[8], G. T. Zorn[17].

[1]School of Physics and Space Research, University of Birmingham, Birmingham B15 2TT, UK
[2]Dipartimento di Fisica dell' Università di Bologna and INFN, I-40126 Bologna, Italy
[3]Physikalisches Institut, Universität Bonn, D-53115 Bonn, Germany
[4]Department of Physics, University of California, Riverside CA 92521, USA
[5]Cavendish Laboratory, Cambridge CB3 0HE, UK
[6]Carleton University, Department of Physics, Colonel By Drive, Ottawa, Ontario K1S 5B6, Canada
[7]Centre for Research in Particle Physics, Carleton University, Ottawa, Ontario K1S 5B6, Canada
[8]CERN, European Organisation for Particle Physics, CH-1211 Geneva 23, Switzerland
[9]Enrico Fermi Institute and Department of Physics, University of Chicago, Chicago IL 60637, USA
[10]Fakultät für Physik, Albert Ludwigs Universität, D-79104 Freiburg, Germany
[11]Physikalisches Institut, Universität Heidelberg, D-69120 Heidelberg, Germany
[12]Indiana University, Department of Physics, Swain Hall West 117, Bloomington IN 47405, USA
[13]Queen Mary and Westfield College, University of London, London E1 4NS, UK
[14]Birkbeck College, London WC1E 7HV, UK
[15]University College London, London WC1E 6BT, UK
[16]Department of Physics, Schuster Laboratory, The University, Manchester M13 9PL, UK
[17]Department of Physics, University of Maryland, College Park, MD 20742, USA
[18]Laboratoire de Physique Nucléaire, Université de Montréal, Montréal, Quebec H3C 3J7, Canada
[19]University of Oregon, Department of Physics, Eugene OR 97403, USA
[20]Rutherford Appleton Laboratory, Chilton, Didcot, Oxfordshire OX11 0QX, UK
[21]CEA, DAPNIA/SPP, CE-Saclay, F-91191 Gif-sur-Yvette, France
[22]Department of Physics, Technion-Israel Institute of Technology, Haifa 32000, Israel
[23]Department of Physics and Astronomy, Tel Aviv University, Tel Aviv 69978, Israel
[24]International Centre for Elementary Particle Physics and Department of Physics, University of Tokyo, Tokyo 113, and Kobe University, Kobe 657, Japan
[25]Brunel University, Uxbridge, Middlesex UB8 3PH, UK
[26]Particle Physics Department, Weizmann Institute of Science, Rehovot 76100, Israel

[27]Universität Hamburg/DESY, II Institut für Experimental Physik, Notkestrasse 85, D-22607 Hamburg, Germany
[28]University of Victoria, Department of Physics, P O Box 3055, Victoria BC V8W 3P6, Canada
[29]University of British Columbia, Department of Physics, Vancouver BC V6T 1Z1, Canada
[30]University of Alberta, Department of Physics, Edmonton AB T6G 2J1, Canada
[31]Duke University, Dept of Physics, Durham, NC 27708-0305, USA
[32]Technische Hochschule Aachen, III Physikalisches Institut, Sommerfeldstrasse 26-28, D-52056 Aachen, Germany

[a]Also at TRIUMF, Vancouver, Canada V6T 2A3

1 Introduction

The dynamics of a gauge theory, such as Quantum Chromodynamics (QCD), are completely defined by the commutation relations between its group generators T^i:

$$\left[T^i , T^j \right] = i \sum_k f^{ijk} \cdot T^k \quad , \tag{1}$$

where the coefficients f^{ijk} are the structure constants, and the generators T^i can be represented as matrices. The generators and structure constants appear in the vertex functions of Feynman graphs. In perturbative calculations, the average and sum over all possible colour configurations in, respectively, the initial and final states lead to the appearance of combinatoric factors C_F, C_A and T_F [1], where

$$
\begin{aligned}
\sum_{k,\eta} T_{\alpha\eta}^k T_{\eta\beta}^k &= \delta_{\alpha\beta} C_F \\
\sum_{j,k} f^{jkm} f^{jkn} &= \delta^{mn} C_A \\
\sum_{\alpha,\beta} T_{\alpha\beta}^m T_{\beta\alpha}^n &= \delta^{mn} T_F \quad .
\end{aligned}
\tag{2}
$$

These quantities, known as the colour factors, are physical manifestations of the underlying group structure. In the case of strong interactions, they represent the relative strengths of the processes $q \rightarrow qg$, $g \rightarrow gg$ and $g \rightarrow q\bar{q}$, respectively. Measurements of the ratios between the colour factors, for instance C_A/C_F and T_F/C_F, are sufficient to distinguish between different gauge groups. For a theory based on SU(3), such as QCD, these ratios have values of $C_A/C_F = 9/4$ and $T_F/C_F = 3/8$. For the Abelian gluon model U(1)$_3$, from which gluon self-couplings are absent, they are $C_A/C_F = 0$ and $T_F/C_F = 3$. For the non-Abelian group SO(3), $C_A/C_F = T_F/C_F = 1$.

A simultaneous measurement of the ratios C_A/C_F and T_F/C_F at e$^+$e$^-$ colliders is possible through the study of angular correlations in four-jet events. Previous studies of four-jet events by the OPAL, L3 and VENUS Collaborations, using angular observables sensitive to T_F/C_F, have shown the experimental results to be incompatible with the Abelian gluon model [2, 3, 4]. Subsequently, the DELPHI and ALEPH Collaborations have published measured values of C_A/C_F and T_F/C_F [5, 6, 7].

In this paper, we present new measurements of C_A/C_F and T_F/C_F. The data were collected with the OPAL detector at the LEP e$^+$e$^-$ collider. Values of C_A/C_F and T_F/C_F are extracted from a fit of theory to data using a three-dimensional distribution of three angular variables constructed from four-jet event data. A review of the theoretical basis for this study is given in section 2. In section 3, we present a brief account of the OPAL detector and the data sample used in this analysis. In section 4, we describe the jet algorithm and four-jet event selection procedure. Our measurement of the colour factor ratios and the evaluation of systematic uncertainties are discussed in sections 5 and 6. Our final results are presented in section 7. Section 8 contains a discussion and summary.

2 Theoretical basis

Within the framework of QCD, four-jet events can occur in e^+e^- annihilations through two basic processes: $e^+e^- \to q\bar{q}gg$ and $e^+e^- \to q\bar{q}q\bar{q}$. The differential four-jet cross section is therefore:

$$d\sigma_4(y_{ij}) = d\sigma_{q\bar{q}gg}(y_{ij}) + d\sigma_{q\bar{q}q\bar{q}}(y_{ij}) \quad , \qquad (3)$$

where $y_{ij} = (p_i + p_j)^\mu (p_i + p_j)_\mu / s$ are normalised two-body invariant masses, with indices i and j running over the four partons. To order α_S^2, the $e^+e^- \to q\bar{q}gg$ term includes contributions from eight tree-level graphs, divided into three classes: the double-bremsstrahlung (DB) graphs of figures 1(a) and 1(b), and the triple-gluon vertex (TGV) graph of figure 1(c). The resulting differential cross section can be expressed as a sum of three terms in which the colour factors appear only as coefficients accompanying group-independent kinematic functions $A(y_{ij})$, $B(y_{ij})$, and $C(y_{ij})$ [8]:

$$\frac{1}{\sigma_0} d\sigma_{q\bar{q}gg}(y_{ij}) = \left(\frac{\alpha_S C_F}{\pi} \right)^2 \left[A(y_{ij}) + \left(1 - \frac{1}{2}\frac{C_A}{C_F} \right) B(y_{ij}) + \frac{C_A}{C_F} C(y_{ij}) \right] d\tilde{y}_{ij} \quad . \qquad (4)$$

In the above equation, σ_0 denotes the Born cross section for the process $e^+e^- \to q\bar{q}$, and $d\tilde{y}_{ij}$ the product of the differentials of any five of the six y_{ij} variables (for example, $dy_{12}dy_{13}dy_{14}dy_{23}dy_{24}$). Loosely speaking, $A(y_{ij})$ in the above expression is the contribution of the DB graphs, $C(y_{ij})$ is that of the TGV graph, and $B(y_{ij})$ is the interference term. More rigorously, while $A(y_{ij})$ does contain the self-squared terms from all of the DB graphs and $C(y_{ij})$ those of the TGV graphs, all three contain interference terms between the eight contributing graphs.

The $e^+e^- \to q\bar{q}q\bar{q}$ process also has eight contributing graphs, all belonging to the class shown in figure 1(d). The differential cross section calculated from these graphs can also be written in a factorised form:

$$\frac{1}{\sigma_0} d\sigma_{q\bar{q}q\bar{q}}(y_{ij}) = \left(\frac{\alpha_S C_F}{\pi} \right)^2 \left[N_F \frac{T_F}{C_F} D(y_{ij}) + \left(1 - \frac{1}{2}\frac{C_A}{C_F} \right) E(y_{ij}) \right] d\tilde{y}_{ij} \quad , \qquad (5)$$

where $D(y_{ij})$ and $E(y_{ij})$ are group-independent kinematic functions, and N_F is the number of active quark flavours.

The relative contributions of the five terms $A(y_{ij}) \ldots E(y_{ij})$ depend on the actual gauge group and on the infra-red cut-off by which jets are defined. In this study, we employ an invariant mass jet-finder, described below, for which there is a single resolution parameter, y_{cut}. Over a wide range of y_{cut} values, the integrals of $A(y_{ij})$, $B(y_{ij})$ and $C(y_{ij})$ are comparable in size, while that of $D(y_{ij})$ is about a factor of five smaller, and $E(y_{ij})$ yet another factor of five smaller than $D(y_{ij})$. Folding in the colour factors, the contribution of $E(y_{ij})$ is negligible compared to that of $D(y_{ij})$ for most known groups, so that the fraction of four-quark events in four-jet events is, to high accuracy, proportional to $N_F T_F / C_F$; the product $N_F T_F$ is often abbreviated to T_R.

The group-independence of $A(y_{ij}) \ldots E(y_{ij})$, and the form of the cross section expressions (4) and (5), imply that the ratios C_A/C_F and T_R/C_F can be determined experimentally by

fitting a linear combination of these five functions to the y_{ij} distributions constructed from data. Equivalently, the experimental distribution of any variable, ζ, which is sensitive to differences between the kinematic functions $A(y_{ij}) \ldots E(y_{ij})$, can be used in a fit of the theoretical distributions $A(\zeta) \ldots E(\zeta)$ to obtain the colour factor ratios.

In this study, we employed the second of the two methods above, extracting values for C_A/C_F and T_R/C_F from a fit of the second-order matrix element calculation to data using a three-dimensional distribution of three angular variables which are sensitive to the QCD group structure. Labelling jets in order of descending energy, such that jet 1 has the highest energy and jet 4 the lowest energy, these three variables are:

(a) the Bengtsson-Zerwas correlation [9], $\cos\chi_{BZ}$, which is the absolute value of the cosine of the angle between the plane spanned by jets 1 and 2 and that by jets 3 and 4,

$$\cos\chi_{BZ} = \left| \frac{(\vec{p_1} \times \vec{p_2}) \cdot (\vec{p_3} \times \vec{p_4})}{|\vec{p_1} \times \vec{p_2}| \, |\vec{p_3} \times \vec{p_4}|} \right| \quad ; \tag{6}$$

(b) the modified Nachtmann-Reiter variable [10], $|\cos\theta^*_{NR}|$, which is the absolute value of the cosine of the angle between the vectors $\vec{p_1} - \vec{p_2}$ and $\vec{p_3} - \vec{p_4}$,

$$|\cos\theta^*_{NR}| = \left| \frac{(\vec{p_1} - \vec{p_2}) \cdot (\vec{p_3} - \vec{p_4})}{|\vec{p_1} - \vec{p_2}| \, |\vec{p_3} - \vec{p_4}|} \right| \quad ; \qquad \text{and} \tag{7}$$

(c) $\cos\alpha_{34}$ [5], the cosine of the angle between the two lowest energy jets,

$$\cos\alpha_{34} = \frac{\vec{p_3} \cdot \vec{p_4}}{|\vec{p_3}| \, |\vec{p_4}|} \quad . \tag{8}$$

Figures 2(a), (b) and (c) show, for the three variables, the theoretical distributions for events from the five kinematic classes corresponding to $A(y_{ij}) \ldots E(y_{ij})$[1]. It is seen from figures 2(a) and 2(b) that the distributions from classes D and E are markedly different from the corresponding distributions from classes A, B and C. These two variables are therefore sensitive to variations in T_R/C_F. In the last plot, figure 2(c), both $C(\cos\alpha_{34})$ and $D(\cos\alpha_{34})$ are seen to behave differently from the other distributions, so that $\cos\alpha_{34}$ is sensitive to both C_A/C_F and T_R/C_F [5]. The three selected variables are not entirely independent of each other. For the event selection used in this study, the correlation coefficients $\rho(\cos\chi_{BZ}, |\cos\theta^*_{NR}|)$, $\rho(\cos\chi_{BZ}, \cos\alpha_{34})$, and $\rho(|\cos\theta^*_{NR}|, \cos\alpha_{34})$, have values of 0.66, 0.18 and 0.29, respectively.

3   Detector and data sample

A detailed description of the OPAL detector is found elsewhere [11]. For this study, we use information from the central tracking detector and the electromagnetic calorimeter.

---

[1]These distributions were obtained from the parton-level Monte Carlo discussed in section 5.1.

The tracking of the charged particles is performed with the central detector, which contains a silicon microvertex detector [12] and three systems of drift chambers: an inner vertex chamber, a large volume jet chamber, and specialised chambers at the outer radius of the jet chamber used to improve position measurements in the z-direction[2]. The tracking chambers are enclosed by a solenoidal magnet providing an axial field of approximately 0.435 T. Most of the tracking information is provided by the jet chamber, which gives up to 159 space points per track and nearly 100% track-finding efficiency in the region $|\cos\theta| < 0.92$. The momentum resolution for charged tracks is $\Delta p/p \approx 5\%$ at $p \approx 45$ GeV/c. The average angular resolution is approximately 0.1 mrad in ϕ and 1 mrad in θ.

Electromagnetic energy is measured using an array of lead-glass blocks located outside the magnet coil, separated into a barrel ($|\cos\theta| < 0.82$), and two end-cap ($0.81 < |\cos\theta| < 0.98$) sections. Each block provides an angular coverage of roughly 40×40 mrad^2, and a depth of about 25 radiation lengths to the back of the calorimeter. Contiguous blocks with energy deposition above threshold are grouped into clusters. Clusters in the barrel that match extrapolated track coordinates at the entrance to the calorimeter to within 80 mrad in ϕ and 150 mrad in θ are associated with a charged track, and are excluded to avoid double-counting of energy. A corresponding cut is made on clusters in the end-caps, but with limits of 50 mrad in both ϕ and θ.

The analysis presented in this paper is based on 1 105 045 Z^0 hadronic decays collected by OPAL during 1991 and 1992, corresponding to a total integrated luminosity of about 35 pb^{-1}. Specifications of the OPAL trigger system and the online event selection are found in references [13] and [14], respectively. For the geometrical region used in this study, the selection efficiency is better than 99.6%. In addition, standard quality cuts are made on the tracks and clusters. Each charged track is required to have (a) at least 20 measured points in the jet chamber, (b) transverse momentum in the $r - \phi$ plane greater than 0.15 GeV/c, (c) $|\cos\theta| < 0.94$, (d) distance of closest approach to the origin in the $r - \phi$ plane of no more than 5 cm, and (e) χ^2 per degree-of-freedom of less than 100 for the track fit in the $r - \phi$ plane. Apart from being unassociated with charged tracks, electromagnetic clusters must also span at least two lead-glass blocks, and have a minimum total deposited energy of 0.1 GeV in the barrel section, or 0.3 GeV in the end-cap sections. Accepted charged tracks and clusters are treated like individual particles in the subsequent analysis. Charged tracks are assigned the pion mass, and clusters are treated as photons. Finally, each event is required to have at least five charged tracks in order to reduce contamination from $e^+e^- \rightarrow \tau^+\tau^-$ events.

4   Four-jet event selection

The selection of four-jet events is performed in three steps. First, we use an invariant mass jet-finding algorithm to define jets. Starting by assigning each particle to be an individual jet,

---

[2]The standard OPAL coordinate system is defined so that z is the coordinate parallel to the e^+e^- beam axis, r is the coordinate normal to the beam axis, ϕ is the azimuthal angle and θ is the polar angle with respect to z.

the rescaled invariant mass $\hat{s}_{ij}$ is calculated for each jet pair:

$$\hat{s}_{ij} = \frac{2E_i E_j \cdot (1 - \cos\theta_{ij})}{E_{vis}^2} \quad , \tag{9}$$

where E_{vis} is the sum of the energies of the accepted particles, E_i is the energy of jet i (initially the energy of an individual particle), and θ_{ij} is the angle between jets i and j. The pair with the smallest value of $\hat{s}_{ij}$ is combined into a single jet k, where the momentum vector $\vec{p}_k$ and energy E_k of the new jet are given by

$$\begin{aligned} \vec{p}_k &= \vec{p}_i + \vec{p}_j \\ E_k &= |\vec{p}_k| \quad . \end{aligned} \tag{10}$$

This method of combining jets is known as the JADE-P0 scheme [15, 16]. The $\hat{s}_{ij}$ values are then recalculated for the remaining jets. This procedure is repeated until exactly four jets remain. The polar angle θ_i of each jet in the event is required to lie in the range $|\cos\theta_i| < 0.90$. In order to reduce background from poorly reconstructed events, each jet is required to contain at least three particles, and to have a minimum visible energy, $(E_i^v)_{\min}$, of 3 GeV. The visible energy of a jet, E_i^v, is found by summing the energies of the particles assigned to the jet.

Second, the polar and azimuthal angles, (θ_i, ϕ_i), of the jet momentum vectors $\vec{p}_i$ are used to obtain a more precise determination of the jet energies. This process makes use of four-momentum conservation, and assumes the jets to represent massless partons, leading to a four-dimensional matrix equation in which the calculated jet energies, E_i^c, appear as the unknowns to be solved. This procedure is essentially the three-dimensional analogue of the method of calculating jet energies from opening angles in three-jet events (see, for instance, reference [17]).

Third, we apply a lower acceptance limit of $y_{cut} = 0.03$ on the normalised invariant mass, y_{ij}, determined from θ_{ij} and E_i^c for each pair of jets,

$$y_{ij} \equiv \frac{2E_i^c E_j^c \cdot (1 - \cos\theta_{ij})}{E_{cm}^2} > y_{cut} \quad , \tag{11}$$

with E_{cm} the centre-of-mass energy. This value of y_{cut} is chosen because it results in well separated jets, while still yielding reasonable event statistics. As a systematic check, we also tested other values of y_{cut} (section 6). In both the first and third steps, the JADE-P0 metric is used for the combination of jets. This particular scheme is chosen for two reasons: it gives excellent angular resolution for the jets, and it corresponds closely to the metric used for merging partons in the theoretical calculation we employ [18].

A total of 22 106 events are selected following the above prescription. This three-stage procedure has the advantage of allowing us to incorporate the calculated jet energies directly into the event selection. This feature serves to reduce hadronisation and detector corrections in the analysis, as discussed in section 5.3.

The sample of events selected using this procedure contains five-jet events. To identify these five-jet events, the jet-finder is applied once more as in the first step of the selection procedure

described above, but stopping jet combination when five jets remain. The normalised invariant mass, y_{ij}, is calculated for each of the ten pairs of jets in the same manner as in equation (11), except that the visible energies E_i^v are used in place of E_i^c, and the event visible energy E_{vis} is used in place of E_{cm}, since the technique of calculated jet energies cannot be extended to a five-body problem. Those events for which the minimum normalised invariant mass exceeds $y_{cut} = 0.03$ are identified as five-jet events and are eliminated from the sample. A total of 374 such events are found, leaving 21 732 four-jet events for this study.

5 Analysis

For the extraction of the colour factor ratios C_A/C_F and T_R/C_F, we choose as our theoretical reference the distributions generated directly from the differential cross sections given in equations (4)-(5). These theoretical distributions are obtained from a parton level Monte Carlo calculation. The measured distributions are corrected for the effects of hadronisation and the detector before being fitted by the theory. A brief outline of the analysis procedure is given in the following paragraph, followed by a more detailed description.

First, having ordered the jets in descending order in the calculated energy E_i^c, the vector of observables, $\vec{v} = (\cos \chi_{BZ}, \; |\cos \theta_{NR}^*| , \; \cos \alpha_{34})$, is computed for each measured event and entered into a three-dimensional histogram, $R(\vec{v})$. Next, we apply bin-by-bin corrections for hadronisation and detector distortions. The correction functions are obtained from Monte Carlo (MC) events based on second order QCD. The contents of the data distribution $R(\vec{v})$ are multiplied by the correction function values to yield the corrected data distribution, $T(\vec{v})$. Finally, $T(\vec{v})$ is fitted by a linear combination of the reference distributions $A(\vec{v}) \ldots E(\vec{v})$, obtained from the parton level MC sample. The accompanying coefficients are constrained to have the same form as they appear in equations (4)-(5), leaving C_A/C_F, T_R/C_F and the overall normalisation as the fit parameters.

5.1 Monte Carlo simulation

For this study, $q\bar{q}$, $q\bar{q}g$, $q\bar{q}gg$ and $q\bar{q}q\bar{q}$ events are generated according to the Ellis-Ross-Terrano matrix element calculation (ERT-ME), implemented in JETSET version 7.3 [18]. In this implementation, infra-red divergence of gluon radiation is handled by an invariant mass cut between partons, using a jet combination scheme analogous to the JADE-P0 one [19]. The ERT calculation neglects parton masses and therefore does not distinguish between different quark flavours. This omission is partially remedied in JETSET: quark flavours are assigned to quarks according to calculated probabilities, quark masses are included by rescaling the momenta of quark jets, and those events falling outside of the phase-space region allowed for massive quarks are reassigned to be two-jet events. This procedure is known to give a reasonable approximation of the expected mass suppression [18].

The generation of four-parton events in JETSET is performed using a standard acceptance-rejection technique. The actual value of each term of the differential cross section in equations (4)-(5) is therefore available. For use in this analysis, a small addition is made to the standard JETSET code in order to write out the partial weights $w_A \ldots w_E$, which correspond to the contribution of the five terms for each event generated. These weights are normalised such that $w_A + w_B + w_C = 1$, $w_D = w_E = 0$ for q$\bar{\text{q}}$gg events, and $w_A = w_B = w_C = 0$, $w_D + w_E = 1$ for q$\bar{\text{q}}$q$\bar{\text{q}}$ events. This choice of normalisation allows us to extract the theoretical reference distributions $A(\vec{v}) \ldots E(\vec{v})$. The distribution of $B(\vec{v})$, for example, is constructed by entering $\vec{v}$ from each event into a histogram with weight w_B.

All MC events are generated assuming standard SU(3) colour factors, with an invariant mass limit of $y_{cut} = 0.01$, which is the smallest value allowed in JETSET. A renormalisation scale of $x_\mu^2 \equiv \mu^2/E_{cm}^2 = 1$ is known to give only about half the expected rate of four-jet events if $\alpha_S(\mu)$ is derived from the three-jet rate [20]. To avoid the resulting over-estimation of two- and three-jet background in the simulated event sample, an optimised renormalisation scale of $x_\mu^2 = 0.002$ (default in JETSET) is used instead, to generate the correct proportion of two-, three- and four-jet events [21]. We note that as far as four-jet events are concerned, only the production rate and not the internal structure is affected by the choice of μ.

For the construction of the reference distributions and the numerator distribution for the correction function, we select only four-parton events from the MC. Using the directions of the partons, we determine the calculated energies E_i^c and apply a cut at $y_{cut} = 0.03$, following the last two steps in section 4. For use in the final fit, each reference distribution is divided by the value of its accompanying coefficient in equations (4)-(5), corresponding to the SU(3) colour factors assumed for the simulation. For example, the distributions accumulated for both $B(\vec{v})$ and $E(\vec{v})$ are divided by $\left[1 - \frac{1}{2}(C_A/C_F)\right] = -0.125$. We thus obtain the group independent reference distributions $A(\vec{v}) \ldots E(\vec{v})$ needed for the fit.

To construct the denominator distribution for the correction function, MC events are hadronised according to the Lund string model [22] in JETSET, using parameters tuned simultaneously to OPAL measurements of event shapes and the asymmetry of the energy-energy correlation function at $x_\mu^2 = 0.002$ [23]. These hadronic events are then passed through the OPAL detector simulation program [24]. The resulting events are subjected to the same analysis and selection procedures as the data.

5.2 Data correction

To correct for detector and hadronisation effects, a simple bin-by-bin technique is employed. A correction function f_{ijk}^{corr} is constructed for each bin (i, j, k) of the three-dimensional data histogram, R_{ijk}, using the MC samples discussed in section 5.1. If P_{ijk} and Q_{ijk} are the MC predictions for the contents of bin (i, j, k) at the parton and detector levels, respectively, after normalisation to the same number of events, then the correction function is given by

$$f_{ijk}^{corr} = \frac{P_{ijk}}{Q_{ijk}} \quad . \tag{12}$$

The corrected data distribution T_{ijk} is then

$$T_{ijk} = f_{ijk}^{corr} \cdot R_{ijk} \quad . \tag{13}$$

The three-dimensional distribution of the variables $\cos \chi_{BZ}$, $|\cos \theta_{NR}^*|$ and $\cos \alpha_{34}$ used in our analysis is formed by dividing each variable range into eight equally-spaced bins. This bin spacing is chosen because it corresponds roughly to the estimated experimental resolution for measuring each of the three variables. Due to partial correlations between the three variables (especially between $\cos \chi_{BZ}$ and $|\cos \theta_{NR}^*|$), the three-dimensional phase space is restricted, such that 100 of the 512 bins contain no events in either the data or detector-level MC. These bins are excluded from the fit. The values of f_{ijk}^{corr} for the other 412 bins are shown by the solid histogram in figure 3. The distribution is seen to be peaked near unity and to be roughly Gaussian, with tails extending to lower and higher values. These tails correspond to regions where the acceptance drops off sharply at the detector level. To eliminate these regions, those bins for which f_{ijk}^{corr} is less than 0.7 or greater than 1.3 are excluded. Most of the 66 bins so excluded are found in the region $\cos \chi_{BZ} > 0.875$, corresponding to the peak at the right edge of figure 2(a) where the four jets are nearly coplanar. Of the remaining 346 bins, a further 51 are rejected because they contain fewer than seven events in the data distribution. A repeat of the fit with these bins restored, and the errors estimated according to Poissonian statistics, does not yield any significant change in the result.

5.3 Effect of using calculated jet energies

In this study, the energies calculated from the directions of the jets, E_i^c, are used both to compute y_{ij} values for the four-jet event selection, and to order the jets in energy for the evaluation of $\cos \chi_{BZ}$, $|\cos \theta_{NR}^*|$ and $\cos \alpha_{34}$. Being less sensitive to detector inefficiencies, hadronisation fluctuations, and uncertainties in the assignment of particles, the calculated energies E_i^c give a more reliable measure of the energies of the four parent partons than the normalised visible jet energies, $\tilde{E}_i^v$, where $\tilde{E}_i^v$ are the visible energies E_i^v introduced in section 4 rescaled such that $\sum_{i=1}^4 \tilde{E}_i^v = E_{cm}$. To illustrate this improvement, we compare E_i^c and $\tilde{E}_i^v$ to the energy of the parent parton in MC events. A one-to-one association of jets to partons is made by selecting the one assignment, out of 24 possible permutations, which minimises $\sum_{i=1}^4 \delta_i^2$, where δ_i is the angle between the ith parton and the jet assigned to it. It is seen in figure 4(a) that the energy resolution is improved by about a factor of two for the two harder jets. However, the improvement between $\tilde{E}_i^v$ and E_i^c is smaller for the two softer jets, as seen in figure 4(b).

The better precision of E_i^c relative to $\tilde{E}_i^v$ offers two advantages. First, the y_{ij} values calculated using E_i^c in equation (11) give a better measure of the y_{ij} between the parent partons than those calculated using $\tilde{E}_i^v$. The event selection at the detector-level is therefore better matched to that at the parton-level when calculated jet energies are used. Second, the use of E_i^c reduces errors in energy ordering in the computation of $\cos \chi_{BZ}$, $|\cos \theta_{NR}^*|$ and $\cos \alpha_{34}$. While these variables are, by construction, invariant under the exchange between jets 1 and 2

11

and between jets 3 and 4, which account for most of the mis-ordering seen in MC events, the better resolution of E_i^c also reduces the residual mis-ordering between one of the two harder jets and one of the two softer jets; the fraction of events where one of the two harder jets is incorrectly identified as one of the two softer jets is reduced from about 30%, when ordering by $\tilde{E}_i^v$, to about 20%, when ordering by E_i^c. Therefore, the use of calculated jet energies also improves the accuracy of the measured $\cos\chi_{BZ}$, $|\cos\theta_{NR}^*|$ and $\cos\alpha_{34}$ values.

The increased precision, both of the event selection and of the energy ordering, combine to reduce the correction for detector and hadronisation effects in this study. This improvement is demonstrated in figure 3, in which we compare the distribution of the values of the correction function, f_{ijk}^{corr}, computed using E_i^c, shown by the solid histogram, to that constructed using $\tilde{E}_i^v$, shown by the dashed histogram. While the latter does show an enhancement near unity, it does not have the well-defined peak seen in the former. This reduction in the correction between the detector- and parton-levels should render our analysis less sensitive to uncertainties in the modelling of the hadronisation process and to inaccuracies in the detector simulation program.

5.4 Extraction of colour factor ratios

To obtain the colour factor ratios C_A/C_F and T_R/C_F, the predicted theoretical distribution, $(T_{ijk})^{pred.}$, given by the weighted sum of the normalised theoretical reference distributions $A_{ijk}\ldots E_{ijk}$, is fitted to the corrected data distribution T_{ijk}.

$$
\begin{aligned}
(T_{ijk})^{pred.} \;=\; & \eta\left\{ A_{ijk} + \left(1 - \frac{1}{2}\frac{C_A}{C_F}\right)B_{ijk} + \frac{C_A}{C_F}C_{ijk} \right. \\
& \left. + \; \frac{T_R}{C_F}D_{ijk} + \left(1 - \frac{1}{2}\frac{C_A}{C_F}\right)E_{ijk}\right\} \quad,
\end{aligned}
\tag{14}
$$

where η is the overall normalisation parameter. The fit is linearised by the following substitutions:

$$
\begin{aligned}
x \;&=\; \eta C_A/C_F \\
y \;&=\; \eta T_R/C_F \\
U_{ijk} \;&=\; A_{ijk} + B_{ijk} + E_{ijk} \\
V_{ijk} \;&=\; C_{ijk} - B_{ijk}/2 - E_{ijk}/2 \quad,
\end{aligned}
\tag{15}
$$

and takes on the standard form

$$
(T_{ijk})^{pred.} = \eta U_{ijk} + x V_{ijk} + y D_{ijk} \quad.
\tag{16}
$$

Minimisation of χ^2 leads to a linear system of three equations in the three variables η, x and y, which can be solved by matrix inversion. From the best-fit values of (η,x,y) and their covariances, values of C_A/C_F, T_R/C_F, and their statistical errors $\sigma_{(C_A/C_F)}$ and $\sigma_{(T_R/C_F)}$ are derived. The covariance matrix element $\sigma_{(C_A/C_F)(T_R/C_F)}^2$ is calculated from

$$
\frac{\sigma_{(C_A/C_F)(T_R/C_F)}^2}{(C_A/C_F)(T_R/C_F)} = \frac{\sigma_\eta^2}{\eta^2} + \frac{\sigma_{xy}^2}{xy} - \frac{\sigma_{\eta x}^2}{\eta x} - \frac{\sigma_{\eta y}^2}{\eta y} \quad.
\tag{17}
$$

Fitting the corrected distribution from data, we obtain a $\chi^2/\text{d.o.f.}$ of $290/292$ and the following values for C_A/C_F, T_R/C_F, their statistical errors, and the correlation parameter $\rho^{stat}_{(C_A/C_F)(T_R/C_F)}$:

$$C_A/C_F = 2.11 \pm 0.16 \qquad\qquad T_R/C_F = 2.01 \pm 0.54$$

(18)

$$\rho^{stat}_{(C_A/C_F)(T_R/C_F)} \equiv \frac{\sigma^2_{(C_A/C_F)(T_R/C_F)}}{\sigma_{(C_A/C_F)}\sigma_{(T_R/C_F)}} = -0.19 \quad .$$

The result of the fit is illustrated in figure 5. The three one-dimensional projections along $\cos\chi_{BZ}$, $|\cos\theta^*_{NR}|$ and $\cos\alpha_{34}$ of the corrected data distribution are shown by the data points, plotted over the projections of the theoretical fit represented by the solid histograms. For purposes of display, the number of bins for figure 5 has been increased beyond the eight per variable used in the fit.

6   Systematic uncertainties

The evaluation of the systematic uncertainties of our measurements included the study of six effects. The results of these systematic studies are summarised in table 1 and a brief description is given in the following paragraphs.

The first effect examined is the uncertainty related to the measurement process and the accuracy of the MC detector simulation. The effect was evaluated by repeating the analysis once using charged tracks alone and a second time using clusters alone for both the data and the detector-level MC sample. For the analysis using charged tracks alone, the same selection criteria as described for the standard analysis were applied. For the analysis using clusters alone, all clusters – both those associated and those unassociated with charged tracks – were used, and a requirement that at least eight clusters be present in an event replaced the requirement of at least five charged tracks: otherwise the selection criteria were the same as those of the standard analysis.

A second uncertainty examined is that associated with the correction procedure. The contribution from this source was evaluated by varying the principal hadronisation parameters of the Monte Carlo, σ_q and a [22]. The analysis was repeated twice. In the first iteration, σ_q was decreased by about 10% from its nominal value, before the correction values f^{corr}_{ijk} were determined, while a was held at its tuned value. In the second iteration, a was increased by about 10% while σ_q was held at its nominal value. These changes correspond roughly to one standard deviation variations in the parameter values allowed for the ERT-ME generator at the Z^0 energy, as found by the LEP experiments [23, 25, 26, 27]. A third parameter, b, is strongly correlated with a, and was therefore kept fixed.

A third uncertainty is due to the possible presence of two- and three-jet-like events in the four-jet sample. This uncertainty was assessed by repeating the analysis using values of 2.0 and 5.0 GeV for the minimum visible jet energy, $(E^v_i)_{\text{min}}$, rather than the value of 3.0 GeV used in

the standard analysis. A smaller value of $(E_i^v)_{\min}$ allows additional two- and three-jet-like events to satisfy the four-jet selection criteria, since a "jet" is more likely to arise as a consequence of fluctuations in the hadronisation and detection processes. To indicate the influence of the $(E_i^v)_{\min}$ value, we counted the number of two- and three-parton events in the detector-level MC which passed the four-jet criteria: we found these events to represent 2.5%, 1.1% and 0.2% of the four-jet MC sample for a $(E_i^v)_{\min}$ value of 2.0, 3.0 and 5.0 GeV, respectively.

In the fourth study, uncertainties related to the jet definition were evaluated by repeating the analysis using the Durham $k_\perp$ [28] and the Luclus [18] jet-finders in the first step of the event selection in section 4, in place of the JADE-P0 one. In particular, Luclus represents a substantially different approach to defining jets compared to the $k_\perp$ and JADE-P0 methods.

Fifth, the uncertainty arising from the bins selected for the fit was evaluated by repeating the analysis using values of the correction function f_{ijk}^{corr} in the ranges $0.5 < f_{ijk}^{corr} < 2.0$ and $0.8 < f_{ijk}^{corr} < 1.2$, in place of the range $0.7 < f_{ijk}^{corr} < 1.3$ used previously.

Last, a potential shortcoming of the ERT matrix element in describing four-jet data is the absence of quark masses. The JETSET implementation of ERT includes the effects of quark masses on the kinematics, as noted in section 5.1, but not on the angular structure of the events it produces. To estimate the influence of finite quark masses on our results, we performed parton level MC studies using the $q\bar{q}gg$, $q\bar{q}q\bar{q}$ generator of Ballestrero, Maina and Moretti (BMM) [29] and the $q\bar{q}gg$, $q\bar{q}\tilde{g}\tilde{g}$ generator of Mũnoz-Tapia and Stirling (MS) [30]. The first of these generators includes quark masses in the matrix element in a general way, while the second includes them for the gluino $\tilde{g}$ only, which is taken to be a massive b quark for the purposes of this analysis [3]. We generated the three-dimensional distribution of $\cos\chi_{BZ}$, $|\cos\theta_{NR}^*|$ and $\cos\alpha_{34}$ using the BMM and MS generators and obtained values for C_A/C_F and T_R/C_F by fitting them following the procedure given in section 5.4, using the ERT formulae for the theoretical reference distributions $A(y_{ij})\ldots E(y_{ij})$ as in our standard analysis. The BMM and MS samples were generated with and without a non-zero value for the b quark mass. The masses of the other quarks were maintained at zero. The b quark mass used was 5 GeV/c^2. For C_A/C_F, the results obtained using BMM and MS remained the same for zero and non-zero b quark masses and were in agreement with the QCD value for this ratio. For T_R/C_F, both the BMM and MS programs predicted a shift downwards of -0.1, relative to the QCD result, if massive b quarks were used in the $q\bar{q}q\bar{q}$ events (for MS, these are $q\bar{q}\tilde{g}\tilde{g}$ events). The BMM program predicted a net upward shift of +0.2 in T_R/C_F, however, if massive b quarks were allowed to appear in the $q\bar{q}gg$ events as well. We conclude that finite quark masses do not affect our results for C_A/C_F, and that the measured T_R/C_F would be shifted by -0.2 if quark masses were included in the theoretical reference distributions.

For all the effects listed above, we follow common practice and define the systematic uncertainty by taking half the full-range deviation observed when the condition was varied, including the standard result presented in section 5.4. The systematic errors so obtained are listed in table 2. The different sources of systematic uncertainty were added in quadrature to define the

---

[3]Gluinos have the same spin as quarks so that the angular structure of $q\bar{q}\tilde{g}\tilde{g}$ events is the same as that of $q\bar{q}q\bar{q}$ events.

total systematic error. For C_A/C_F, the largest uncertainties are associated with the choice of the jet-finder and the estimate of the two- and three-jet background. For T_R/C_F, the largest uncertainties arise from the choice of the jet-finder, the measurement process and the correction procedure. The variations in C_A/C_F and T_R/C_F observed in table 1 were used to evaluate the correlation between the systematic errors of the two colour factor ratios. We obtain:

$$\rho^{sys}_{(C_A/C_F)(T_R/C_F)} = -0.57 \quad .\tag{19}$$

This value is assumed when combining the systematic and statistical uncertainties. The inclusion of this correlation does not affect the error for the individual C_A/C_F and T_R/C_F measurements, but it does affect the confidence level contours if C_A/C_F and T_R/C_F are considered in a two-dimensional space (see section 7).

For completeness, three additional cross-checks were made. First, the analysis was repeated using from six to ten equally spaced bins in each of the three variables, rather than eight bins as in the standard analysis. No significant shifts were seen in the results. Second, the y_{cut} value was varied. While essentially no variation was seen in T_R/C_F, increased y_{cut} values caused a shift toward higher C_A/C_F for the standard track selection. For example, a y_{cut} value of 0.05 (the highest value we tested) resulted in $C_A/C_F = 3.04 \pm 0.47$(stat.). However, this shift was absent when charged tracks alone were used: for $y_{cut} = 0.05$, we found C_A/C_F to be 1.87 ± 0.45(stat.) using charged tracks alone. We interpret this difference between the results found using charged tracks alone or the standard track selection to be an experimental effect already taken into consideration in the above systematic studies. Note that the analysis employing larger y_{cut} values provides an implicit test of the effects of five-jet events on our results, since some of the events which had been classified as five-jet events using $y_{cut} = 0.03$ become classified as four-jet events, and thus enter the experimental distributions. Third, a comparison was made between the results of our standard analysis and those obtained choosing different combinations of $\cos \chi_{BZ}$, $|\cos \theta^*_{NR}|$ and $\cos \alpha_{34}$, combined in two-dimensional fits, rather than a three-dimensional one. The two-dimensional fits were found to yield consistent results with the three-dimensional one.

7   Final results

Combining the individual contributions to the overall systematic error, we obtain:

$$
\begin{aligned}
C_A/C_F &= 2.11 \pm 0.16\,(\text{stat.}) \pm 0.28\,(\text{syst.}) \\
T_R/C_F &= 2.01 \pm 0.54\,(\text{stat.}) \pm 0.68\,(\text{syst.}) \quad .
\end{aligned}\tag{20}
$$

Adding statistical and systematic errors in quadrature, while taking account of correlations between the systematic uncertainties as given in equation (19), and dividing T_R by five active quark flavours, we obtain the following final results:

$$C_A/C_F = 2.11 \pm 0.32 \qquad\qquad T_F/C_F = 0.40 \pm 0.17$$

$$\tag{21}$$

$$\rho_{(C_A/C_F)(T_F/C_F)} = -0.45 \qquad .$$

15

The central values are marked in figure 6 by the star. The 68% and 95% confidence level intervals are bounded by the solid and dashed ellipses, respectively. The predictions of various gauge models are also plotted in the figure. Our result is clearly in agreement with the standard QCD expectations of $C_A/C_F = 9/4$ and $T_F/C_F = 3/8$, indicated by the triangle in the figure. All models shown with open squares and circles are already excluded by the fact that they do not contain three degrees of freedom (colours) for quarks. The only groups other than SU(3) which contain three quark colours are the $U(1)_3$ Abelian gluon model and SO(3), both of which are excluded by this study.

8 Discussion and summary

Four-jet events are selected from hadronic Z^0 decays recorded by the OPAL detector at the LEP e^+e^- collider, using the JADE-P0 jet-finder with a jet resolution cut of $y_{cut} = 0.03$. Three-dimensional distributions are constructed for $\cos\chi_{BZ}$, $|\cos\theta^*_{NR}|$ and $\cos\alpha_{34}$. The experimental distribution of the selected observables is fitted by a linear combination of the theoretical reference distributions generated using a second order matrix element calculation, in which the four-jet state appears at tree level. We find from the fit:

$$C_A/C_F = 2.11 \pm 0.32$$

$$T_F/C_F = 0.40 \pm 0.17 \quad ,$$

(22)

in agreement with QCD predictions of $C_A/C_F = 9/4$ and $T_F/C_F = 3/8$. These results are consistent with those previously reported by the DELPHI and ALEPH Collaborations[7, 6].

Some new features of our analysis are that we employ the technique of calculated jet energies for four-jet events, which improves the jet energy resolution and reduces the hadronisation and detector corrections, and that we investigate the effect of finite quark masses on the matrix element calculation. This analysis also includes several systematic studies not considered previously, such as the effect of using different jet-finders and the evaluation of the measurement errors by repeating our study using charged tracks alone, and electromagnetic clusters alone.

The precision of our results is limited by the systematic uncertainties. Although in good agreement with QCD, our result of $T_F/C_F = 0.40 \pm 0.17$ is not sufficient to exclude the possible existence of a light gluino. Even in the extreme case of a massless gluino, the expected value of $T_F/C_F = 0.6$ [31] (increased from 3/8 by the occurrence of $e^+e^- \rightarrow q\bar{q}\tilde{g}\tilde{g}$ events which mimic the angular structure of four-quark events) lies only slightly beyond the 68% confidence level upper limit of our result. The inclusion of a gluino mass of more than about 2 GeV would bring the expectation to within one standard deviation of the measured value.

9 Acknowledgements

References

[1] C. Quigg, "Gauge Theories of the Strong, Weak, and Electromagnetic Interactions", Benjamin/Cummings (Menlo Park, 1983).

[2] OPAL Collaboration, M. Z. Akrawy *et al.*, Z. Phys. **C49** (1991) 49.

[3] L3 Collaboration, B. Adeva *et al.*, Phys. Lett. **B248** (1990) 227.

[4] VENUS Collaboration, K. Abe *et al.*, Phys. Rev. Lett. **66** (1991) 280.

[5] DELPHI Collaboration, P. Abreu *et al.*, Phys. Lett. **B255** (1991) 466.

[6] ALEPH Collaboration, D. Decamp *et al.*, Phys. Lett. **B284** (1992) 151.

[7] DELPHI Collaboration, P. Abreu *et al.*, Z. Phys. **C59** (1993) 357.

[8] R. K. Ellis, D. A. Ross, and A. E. Terrano, Nucl. Phys. **B178** (1981) 421.

[9] M. Bengtsson and P. Zerwas, Phys. Lett. **B208** (1988) 306.

[10] O. Nachtmann and A. Reiter, Z. Phys. **C16** (1982) 45;
M. Bengtsson, Z. Phys. **C42** (1989) 75.

[11] OPAL Collaboration, K. Ahmet *et al.*, Nucl. Instrum. Methods **A305** (1991) 275.

[12] P.P. Allport *et al.*, Nucl. Instrum. Methods **A324** (1993) 34.

[13] M. Arignon *et al.*, Nucl. Instrum. Methods **A313** (1992) 103.

[14] D. G. Charlton, F. Meijers, T. J. Smith, and P. S. Wells, Nucl. Instrum. Methods **A325** (1993) 129.

[15] OPAL Collaboration, M. Z. Akrawy *et al.*, Z. Phys. **C49** (1991) 375.

[16] Z. Kunszt, P. Nason, G. Marchesini and B. R. Webber, "QCD" in "Z Physics at LEP 1", CERN 89-08, vol. 1, eds. G. Altarelli, R. Kleiss and C. Verzegnassi (Geneva, 1989).

[17] OPAL Collaboration, P. Acton *et al.*, Z. Phys. **C58** (1993) 387.

[18] T. Sjöstrand, "PYTHIA 5.6 and JETSET 7.3: Physics and Manual", CERN-TH.6488/92, 1992.

[19] T. Sjöstrand, private communication.

[20] JADE Collaboration, W. Bartel *et al.*, Z. Phys. **C33** (1986) 23.

[21] T. Sjöstrand *et al.*, "QCD Generators" in "Z Physics at LEP 1", CERN 89-08, vol. 3, eds. G. Altarelli, R. Kleiss and C. Verzegnassi (Geneva, 1989).

[22] B. Andersson, G. Gustafson, G. Ingelman, and T. Sjöstrand, Phys. Rep. **97** (1983) 31.

[23] OPAL Collaboration, P. Acton *et al.*, Phys. Lett. **B276** (1992) 547.

[24] J. Allison *et al.*, Nucl. Instrum. Methods **A317** (1992) 47.

[25] OPAL Collaboration, M. Z. Akrawy *et al.*, Z. Phys. **C47** (1990) 505.

[26] ALEPH Collaboration, D. Buskulic *et al.*, Z. Phys. **C55** (1992) 209.

[27] L3 Collaboration, B. Adeva *et al.*, Z. Phys. **C55** (1992) 39.

[28] S. Catani *et. al.*, Phys. Lett. **B269** (1991) 432;
N. Brown and W. J. Stirling, Z. Phys. **C53** (1992) 629;
S. Bethke, Z. Kunszt, D. E. Soper and W. J. Stirling, Nucl. Phys **B370** (1992) 310.

[29] A. Ballestrero, E. Maina, and S. Moretti, Phys. Lett. **B294** (1992) 425.

[30] R. Muñoz-Tapia and W. J. Stirling, Phys. Rev. **D49** (1994) 3763.

[31] T. Hebbeker, Z. Phys. **C60** (1993) 63.

	$\Delta(C_A/C_F)$	$\Delta(T_R/C_F)$
1. Systematic effects related to the measurement process		
charged tracks only	-0.18	$+0.22$
electromagnetic clusters only	-0.12	$+0.69$
2. Systematic effects related to the correction procedure		
$a = 1.5$, $\sigma_q = 0.37$ GeV	$+0.05$	-0.46
$a = 1.7$, $\sigma_q = 0.42$ GeV	-0.01	$+0.39$
3. Systematic effects related to two- and three-jet background		
$E_i^v \geq 2$ GeV	$+0.19$	$+0.15$
$E_i^v \geq 5$ GeV	-0.14	$+0.19$
4. Systematic effects related to the choice of jet-finder		
Durham ($k_\perp$)	$+0.27$	-0.69
Luclus	-0.10	-0.46
5. Systematic effects related to the bin selection in the fit		
$0.5 < f^{corr} < 2.0$	$+0.10$	-0.18
$0.8 < f^{corr} < 1.2$	$+0.06$	-0.10
6. Systematic effects related to quark mass effects		
quark mass in matrix element	$+0.00$	-0.20

Table 1: Summary of systematic effects. The differences $\Delta(C_A/C_F)$ and $\Delta(T_R/C_F)$ are given relative to the results of our standard analysis, $C_A/C_F = 2.11 \pm 0.16$ (stat.) and $T_R/C_F = 2.01 \pm 0.54$ (stat.).

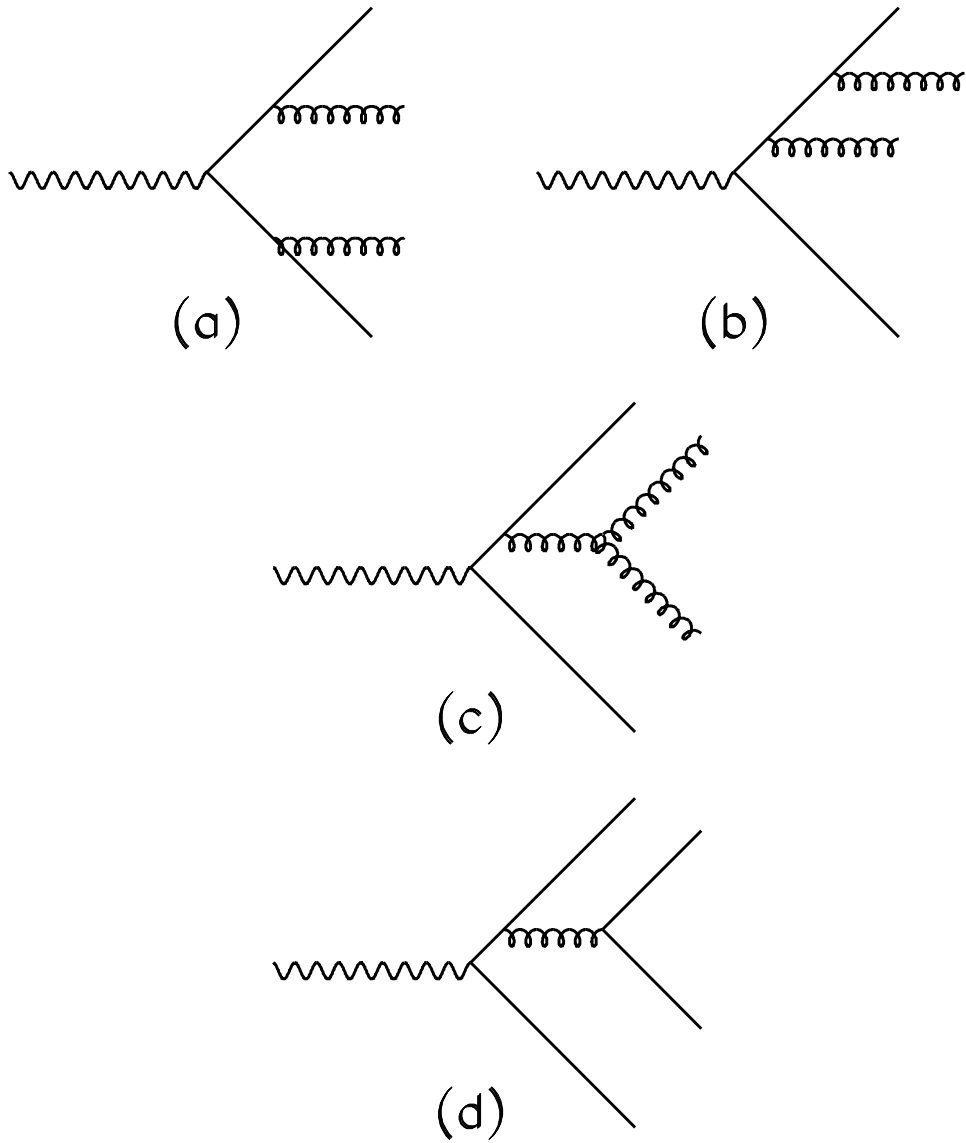| Item	C_A/C_F	T_R/C_F
experimental	0.09	0.35
correction procedure	0.03	0.43
2- & 3-jet background	0.17	0.10
choice of jet-finder	0.19	0.35
bin selection	0.05	0.09
quark mass	0.00	0.10
total systematic error	0.28	0.68

Table 2: Summary of systematic error contributions.

Figure 1: Classes of Feynman graphs contributing to $e^+e^- \to 4$ jets: (a)(b) double gluon bremsstrahlung, (c) triple gluon vertex, (d) $e^+e^- \to q\bar{q}q\bar{q}$.
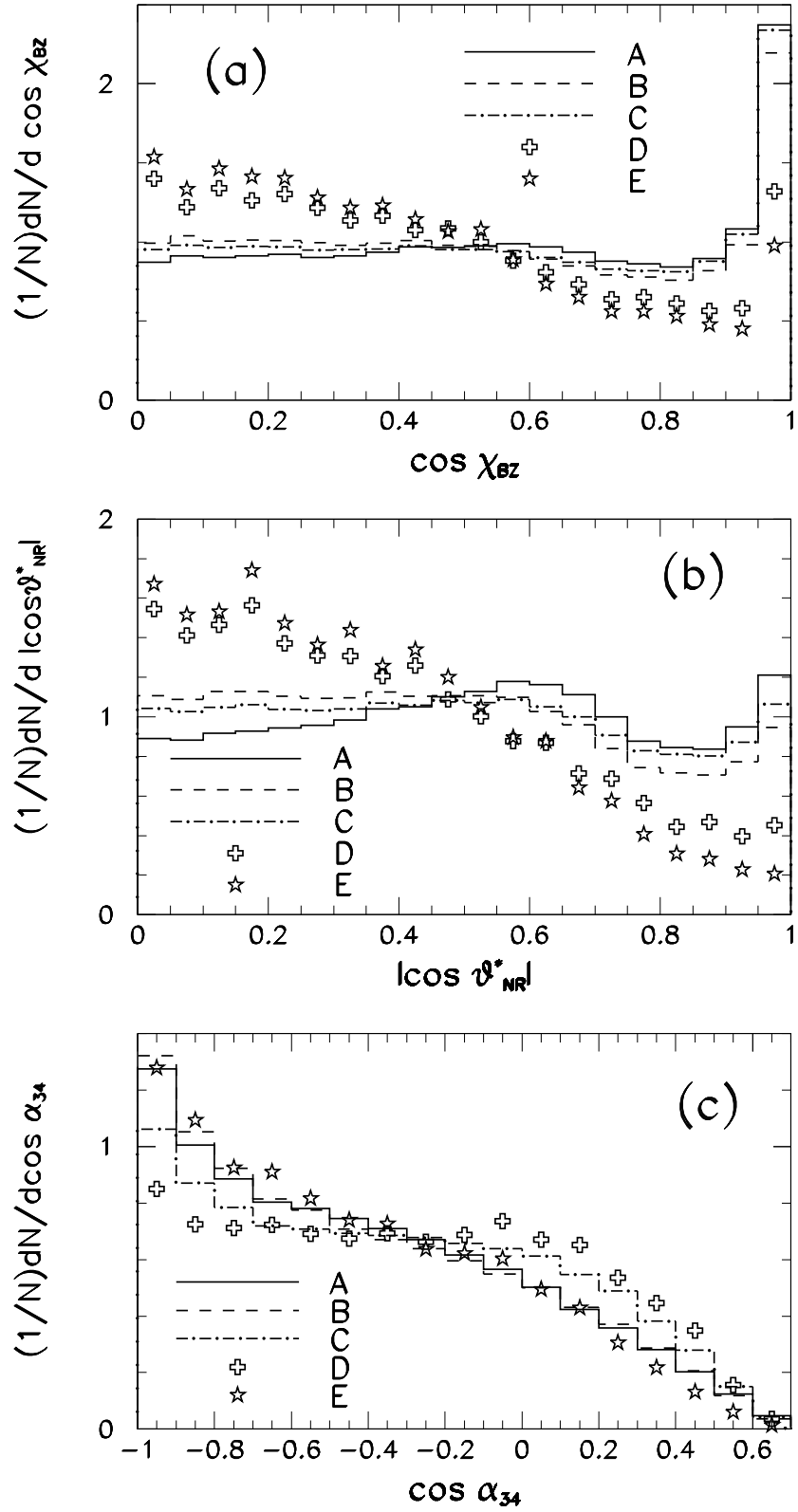
Figure 2: Monte Carlo distributions for (a) $\cos \chi_{BZ}$, (b) $|\cos \theta_{NR}^*|$, and (c) $\cos \alpha_{34}$.
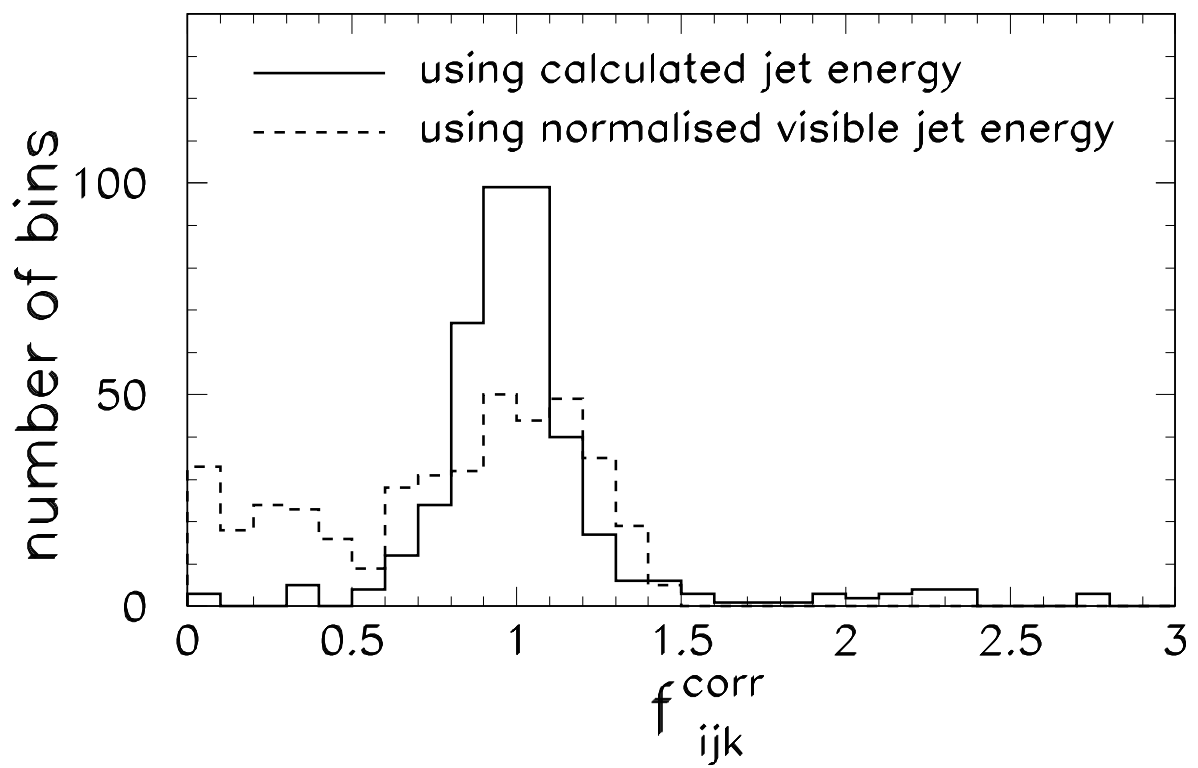
Figure 3: Distributions of correction function values f_{ijk}^{corr} constructed using calculated jet energy (solid histogram) and using normalised visible jet energy (dashed histogram).
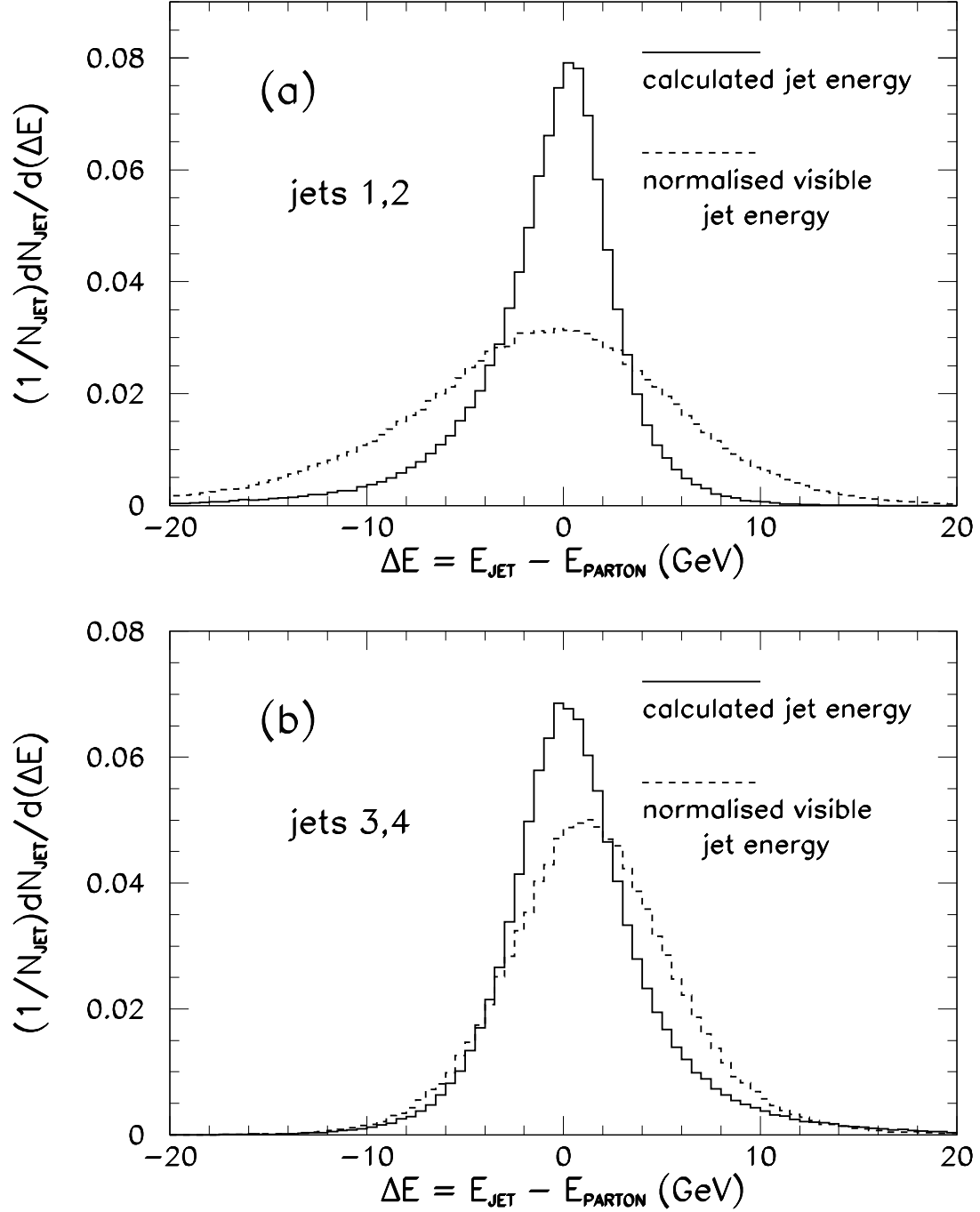
Figure 4: Monte Carlo distributions of the difference between the measured jet energy and the parent parton energy in four-jet events for (a) the two harder jets and (b) the two softer jets. The solid and dashed curves show, respectively, the distributions obtained using calculated jet energies E_i^c, and the those obtained using normalised visible energies $\tilde{E}_i^v$.
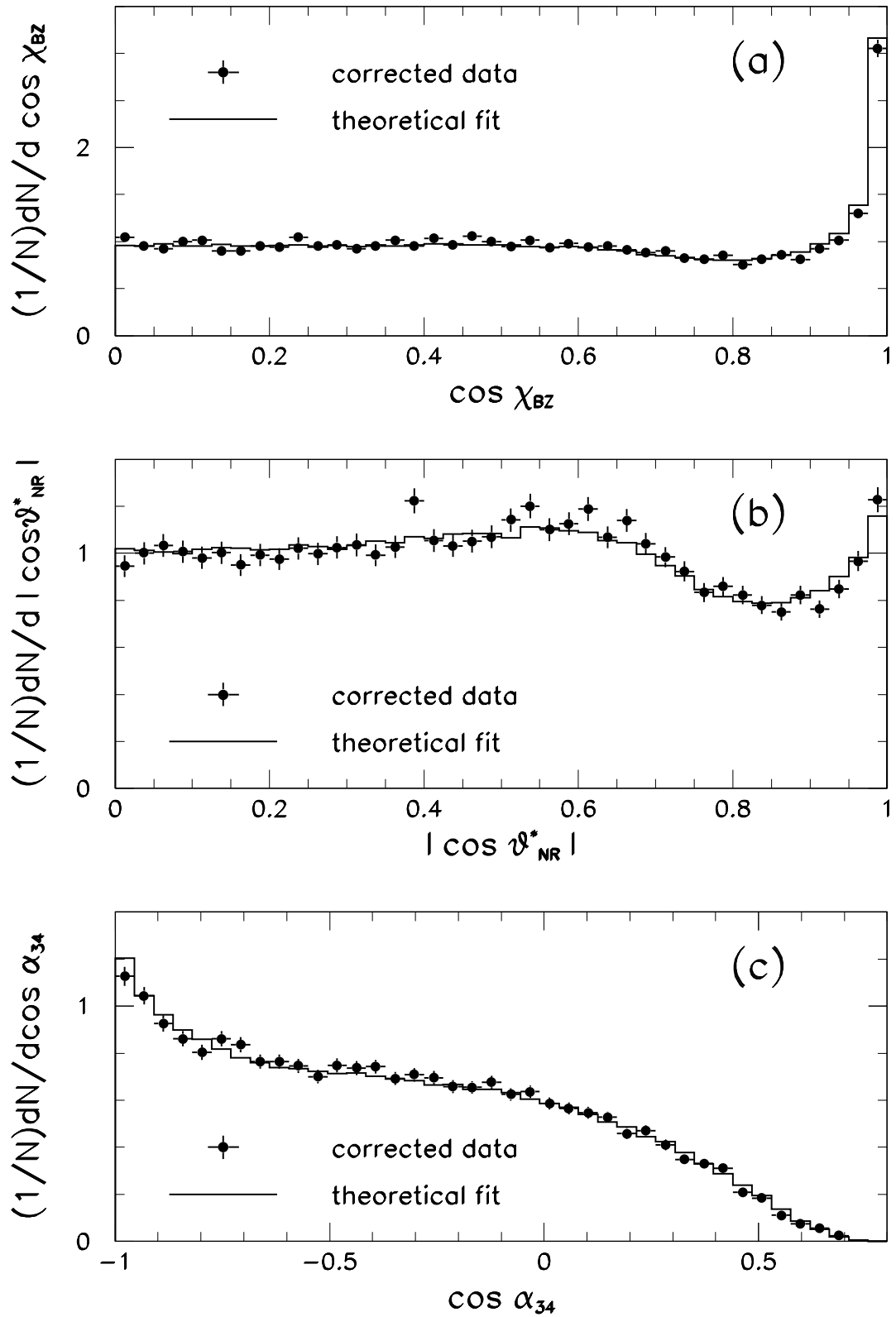
Figure 5: One-dimensional projections along (a) $\cos \chi_{BZ}$, (b) $|\cos \theta^*_{NR}|$, and (c) $\cos \alpha_{34}$ of the corrected data distribution (data points) and of the theoretical fit (solid histogram).
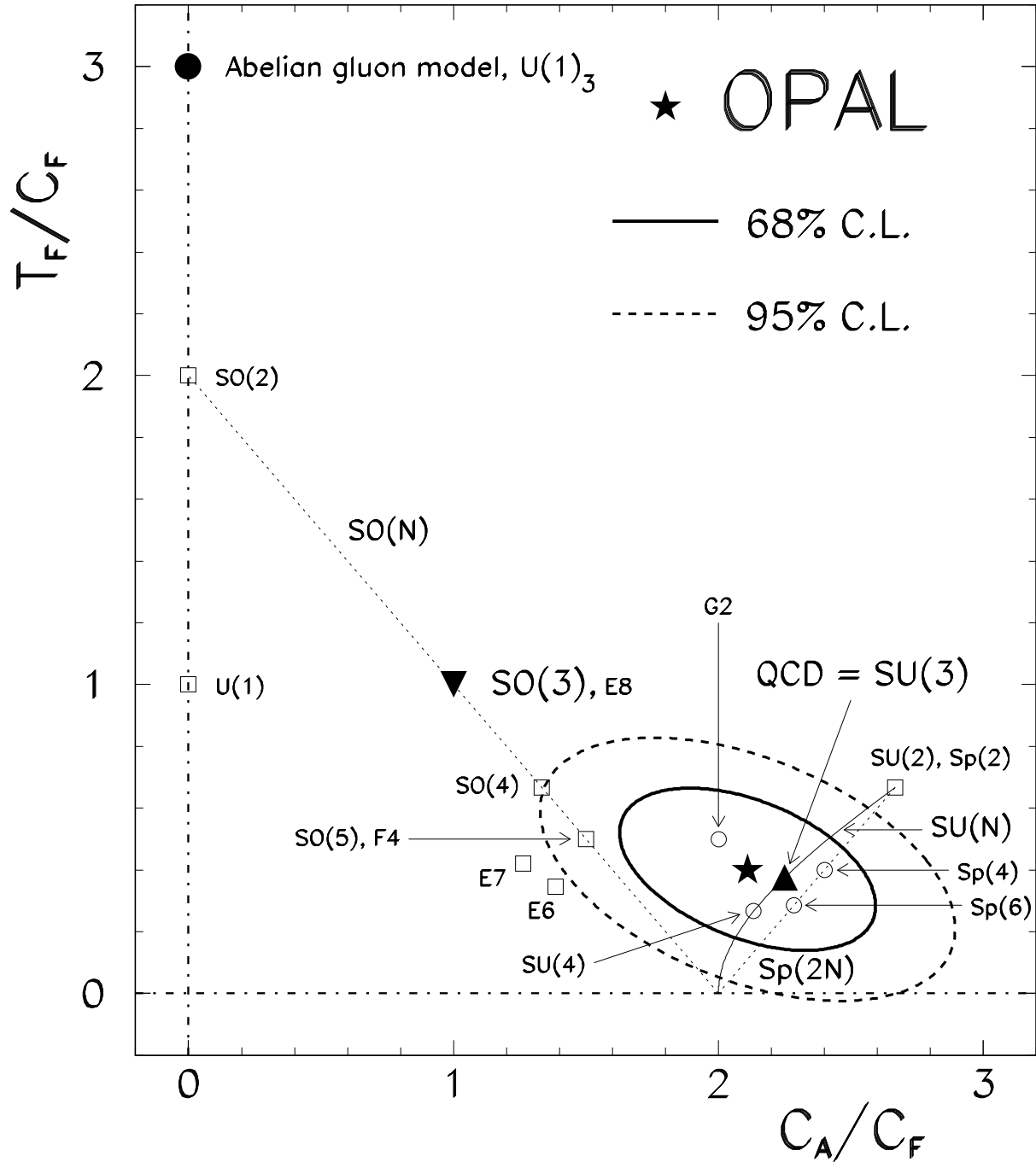
Figure 6: Measured values of colour factor ratios C_A/C_F and T_F/C_F with 68% and 95% confidence-level contours. Expectations from various gauge models are also shown. Those groups shown by the open squares and circles are already excluded because they do not contain three colour degrees of freedom for quarks.